


RESEARCH ARTICLE OPEN ACCESS

In Situ Polymerization of Barium Hexaferrite Ferrofluids for Poly(Ethylene) Succinate Magnetic Nanoparticle Composites

Y. Ahmed¹ | B. D. Ward² | J. Steer¹ | D. Zabek^{1,3} ¹School of Engineering, Cardiff University, Cardiff, UK | ²School of Chemistry, Cardiff University, Cardiff, UK | ³School of Engineering, University of Southampton, Southampton, UK**Correspondence:** D. Zabek (D.A.Zabek@soton.ac.uk)**Received:** 12 November 2024 | **Revised:** 26 February 2025 | **Accepted:** 28 February 2025**Funding:** This work was supported by Royal Academy of Engineering, RF\201819\18\202.**Keywords:** barium hexaferrite | ethylene glycol | ferrofluid | hard magnetic polymer | nanocomposite

ABSTRACT

The integration of hard magnetic barium hexaferrite (BHF) nanoplatelets into a dense poly(ethylene succinate) (PES) polyester matrix produces an exciting biodegradable thermoplastic magnetic polymer nanocomposite. In this work, scandium-substituted BHF nanoplatelets are grown and stabilized in hexadecyltrimethylammonium bromide (CTAB) surfactant and subsequently dispersed in ethylene glycol, producing a stable ferrofluid. The ferrofluid is used for an in situ step-growth condensation polymerization reaction between the ethylene glycol-based ferrofluid and succinic acid. The polymerized ferrofluid forms a hard magnetic nanocomposite with filler content of up to 4.5 wt% of BHF nanoplatelets, which are homogeneously dispersed within a solid polymer matrix. With a filler content 16 times higher than in previous studies, the nanocomposite was chemically analyzed using Fourier Transform Infrared (FTIR) spectroscopy, nuclear magnetic resonance (NMR) spectroscopy, and gel-permeation chromatography (GPC) and optimized for chain length and molecular weight, reaction time and temperature, magnetic moment, and surface hardness. The polymer molecular weight was found to be 1359 g/mol with a monomer-to-polymer conversion of 89%. Highly dense polymer composites were characterized using thermogravimetric analysis (TGA), while magnetic properties were determined by vibrating sample magnetometry (vsm). The synthesized magnetic thermoplastic polymer composite shows excellent magnetic properties, opening the way to advanced 3D magnetic printing and biomedical applications.

1 | Introduction

Magnetic composite materials have magnetic particles embedded in a continuous polymer matrix and combine properties that are not possible in a single phase, such as a hard magnetic moment in a malleable and lightweight polymer structure [1]. Recent advances in magnetic particle and polymer synthesis enable a wider range of applications: three-dimensional (3D) printing [2], self-healing materials [3], environmental and process engineering [4], and biology [5–9]. Magnetic nanocomposites, where at least one geometry dimension is in the nanometer

range, are of particular interest due to the high level of dispersion leading to a homogeneous, or isotropic, composite material. While the dispersed particles exhibit application-specific properties, the polymer matrix also contributes to the material processability and performance [10]. Here, different types of polymer matrix composites (PMCs) are available, such as thermosets, thermoplastics, or rubbers, with thermosetting polymers being the most common. Thermosetting polymers readily form cross-links, or strong covalent bonds between polymer chains, which restrict movement and consequently increase the glass transition temperature to above room temperature

This is an open access article under the terms of the [Creative Commons Attribution](https://creativecommons.org/licenses/by/4.0/) License, which permits use, distribution and reproduction in any medium, provided the original work is properly cited.

© 2025 The Author(s). *Journal of Applied Polymer Science* published by Wiley Periodicals LLC.

and prevent the remodeling of PMCs, which can burn or degrade upon reheating. Thermoplastics differ from thermosets by forming linear polymer chains that do not cross-link and readily flow under stress at high temperatures. This property allows for the remodeling of the PMC and retains the given shape upon cooling to room temperature [11]. Most thermoplastic PMCs are iron oxides or iron-based materials due to their easy preparation and good stability. For iron oxide PMCs, the dispersion and polymer fabrication have been intensively researched for the purpose of improved stability and magnetorheological properties. Guo *et al.* reported improved Fe_3O_4 —PMMA stability through core shells in advanced magnetorheological materials [12, 13]. This produced high magnetic susceptibility and low-density iron oxide PMCs demonstrating a low level of toxicity. Further improvements on biocompatible PMCs were reported for polymer shell-type hybrid particles, which prevent a direct contact between the magnetic nanoparticles and biomolecules, and can also be coated with bioactive targeting molecules [14] for applications in enzyme immobilization [15], magnetic resonance imaging [16], and drug delivery cell separation [17]. In an effort to improve dispersion, magnetic fiber composites were homogeneously dispersed with Fe_3O_4 magnetic nanoparticles in polyvinyl alcohol (PVA) with the help of polyacrylic acid (PAA) acting as a polymer surfactant [18]. Traditionally, these magnetic fibers are produced by coating magnetic nanoparticles onto the surface of the fibers; however, this results in a low magnetic susceptibility due to insufficient amounts of magnetic nanoparticles as well as particle loss after treatment [19]. Similar approaches were reported by incorporating the magnetic nanoparticles directly into a polymeric fiber matrix by mixing; however, the challenge of obtaining well-dispersed nanoparticles without aggregation still remains [20] due to the short-range van der Waals forces and long-range magnetic dipole–dipole interactions between the particles, causing aggregation and effective separation of the two phases [21]. In contrast, isotropic composites can be produced directly from colloidal suspensions through in situ polymerization. Fe_3O_4 magnetic nanoparticles were homogeneously dispersed with a PAA polymer surfactant into Fe_3O_4 /PVA composite materials. However, due to the superparamagnetic properties of Fe_3O_4 , these composites have limited applicability. In contrast, ferrimagnetic barium hexaferrites ($\text{BaFe}_{12}\text{O}_{19}$ or BHF) exhibit a high uniaxial magnetocrystalline anisotropy ($K_1 = 3.3 \times 10^4 \text{ J m}^{-3}$) with the magnetic easy axis parallel to the crystallographic *c*-axis, producing a high coercivity [22] used for permanent magnets, magnetic-recording media, and microwave applications [23]. While ferrimagnetic BHF exhibits high levels of coercivity, the excellent chemical stability, along with the high Curie temperature (450°C) and saturation magnetization ($72 \text{ Am}^2 \text{ kg}^{-1}$) make BHF nanoparticles an excellent filler for polymer composites. Previous studies utilizing in situ polymerization with BHF reported a maximum filler content of 0.27 wt% in PMMA [24]. The filler content of BHF depends mainly on the stability of the colloidal suspension determined by the Brownian motion of the suspended nanoparticles and their geometrical and magnetic-anisotropy [25]. BHF nanoparticles exhibit a hexagonal shape, shown by Went *et al.*, and their diameter depends on the synthesis method used. When in suspension or ferrofluid, BHF nanoparticles also exhibit interesting nematic transitions and domain formations in isotropic liquids [26] and novel magneto-optical properties for magnetic

field visualization [27], or optical coherence tomography [28]. In addition, these ferrofluids potentially have a wide range of commercial applications covering industrial coolants, sealants, light switches, hyperthermia, defect sensors, and drug targeting [29]. For this reason, we utilize ferrimagnetic scandium-substituted barium hexaferrite— $\text{BaFe}_{12}\text{O}_{19}$ nanoparticles in order to produce a novel polymer matrix nanocomposite material with hard magnetic properties. In our work, we coat BHF magnetic nanoparticles with hexadecyltrimethylammonium bromide (CTAB) surfactant, which allows for a stable colloidal dispersion of BHF in ethylene glycol [30]. To take advantage of the high boiling point and functional groups of ethylene glycol solvent, we present a catalyst-free, direct in situ condensation polymerization reaction of the ethylene glycol ferrofluid to produce poly(ethylene) succinate (PES) with embedded barium hexaferrite magnetic nanoplatelets. The PES synthesis for the barium hexaferrite PMC is developed and optimized in this report, followed by the chemical and magnetic characterization of the product. Based on the reported synthesis method, novel direct in situ thermoplastic hard magnetic PMCs are developed with potential applications in three-dimensional (3D) magnetic structures or advanced bioengineering applications.

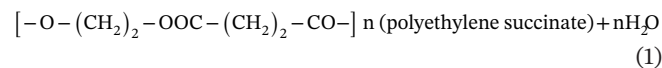
2 | Methodology

2.1 | Synthesis of Magnetic Nanoparticles

Sc-substituted BHF nanoparticles were synthesized using a surfactant-assisted CTAB hydrothermal method at 190°C following a previously reported procedure [31]. The moist CTAB surfactant-coated nanoparticles were dispersed in ethylene glycol (99.8%, Thermo Fisher Scientific) and sonicated for 2 h at 35 W, producing a concentrated BHF ferrofluid.

2.2 | Polymerization of CTAB—Stabilized Ferrofluid

CTAB-stabilized BHF ferrofluid was heated to 170°C in an oil bath with continuous stirring, while succinic acid (99.9%, Thermo Fisher Scientific) was gradually added in a 1:2M ratio (succinic acid to ferrofluid). The ferrofluid mixture was maintained at 170°C with stirring for 10 h, producing PES/BHF and H_2O as follows:



After the product was cooled at room temperature, it produced a solid polyethylene succinate polymer with hard magnetic properties, as illustrated in the graphical abstract. The condensation polymerization reaction between succinic acid monomers and ethylene glycol produces polyethylene succinate and requires the elimination of water to form covalent bonds between the monomers. This catalyst-free and direct in situ condensation polymerization reaction creates a stable thermoplastic PMC while maintaining subsequent dispersion, molecular weight, and magnetic properties over several heating and cooling cycles. The thermoplastic PES is first optimized for the synthesis method with a pure PES matrix, followed by varying the nanoparticles concentration of the PMC. The synthesis of the polyethylene succinate

matrix was optimized for synthesis time and synthesis temperature. For the optimization of the synthesis temperature, ethylene glycol was polymerized with succinic acid at 110°C, 130°C, 150°C, and 170°C. As previous studies [32] have found, the melting point of succinic acid is 184°C, while the boiling point of ethylene glycol and succinic acid is 205°C and 255°C, respectively. For this reason, it is important to stay below the boiling temperature of ethylene glycol and succinic acid, as well as above the boiling temperature of water. The molar ratio of succinic acid and ethylene glycol is also paramount for the polymerization reaction. To determine a suitable molar ratio of the monomers to use, we resorted to previous studies that report the solubility of succinic acid with respect to temperature and conclude that the solubility of succinic acid in all the studied solvents increases with an increase in temperature. Our preliminary studies following a similar protocol confirmed up to 50% succinic acid solubility in ethylene glycol when heated to 80°C (just below the boiling point of water) [33]. The pure PES matrix was characterized using Fourier Transform Infrared (FTIR) spectroscopy, Gel-Permeation Chromatography (GPC), and Nuclear Magnetic Resonance (NMR) spectroscopy to analyze the molecular weight as well as the monomer to polymer conversion as the polycondensation time and temperature were increased. The polymer molecular weight (M_n) was determined using the following equation:

$$M_n = \frac{\sum N_i M_i}{\sum N_i} \quad (2)$$

where N_i is the number of molecules of species i , and M_i is the molecular weight of species i [34]. In addition, surface hardness of the polymers, a key mechanical application property, was also measured with reaction time. After we optimized the pure polymer matrix synthesis, the same method was followed for the polymerization of barium hexaferrite based ferrofluids. Different concentrations of bulk ferrofluid samples were polymerized and characterized using Thermogravimetric Analysis (TGA) and Vibrating Sample Magnetometry (VSM) analysis while microtome sliced samples were prepared for Transmission Electron Microscopy (TEM).

3 | Results and Discussion

According to Figure 1, FTIR analysis confirms for pure PES a successful polymerization reaction between the succinic acid and the ethylene glycol monomers. The main characteristic peaks of succinic acid are 3200–2500 cm^{-1} which correspond to the broad stretching vibration of the O–H group [35]; 2630 and 2530 cm^{-1} are due to the C–H stretching, while the peak at 1689 cm^{-1} corresponds to the C=O group stretching vibration, and the peak at 895 cm^{-1} results from the out-of-plane bending of the bonded –OH group of the carboxylic acid [32]. The peaks at 1411 and 1296 cm^{-1} were due to C–O–H in-plane bending ($\delta_{\text{C–O–H}}$) and C–O stretching vibration, respectively [36]. The FTIR results for ethylene glycol show the main characteristic peaks, which include 3294 cm^{-1} due to the OH group stretching vibration and the peaks at 2939 and 2870 cm^{-1} which are assigned to the asymmetric and symmetric stretching of C–H bonds. The peak at 1388 cm^{-1} results from the CH_2 bending, while nearby peaks correspond to C–O–H bending. The peaks at 1080 and 1033 cm^{-1} are due to the C–O stretching, and the

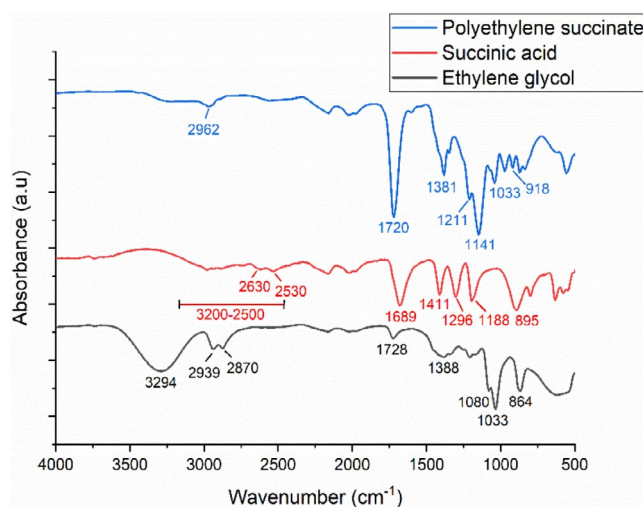


FIGURE 1 | FTIR analysis of ethylene glycol, succinic acid, and pure polyethylene succinate (PES). [Color figure can be viewed at [wileyonlinelibrary.com](https://onlinelibrary.wiley.com/doi/10.1002/app.56984)]

peak at 864 cm^{-1} corresponds to the CH_2 rocking [37]. Most importantly, the peak at 1720 cm^{-1} signifies the formation of the ester bond, which is absent in both monomers, specifically, the C=O group stretching vibration. This is coupled with the disappearance of the C=O group stretching vibration of succinic acid and the OH group stretching vibration of ethylene glycol, which also confirms a successful condensation polymerization reaction. Additionally, for pure PES, peaks at 1141 and 1211 cm^{-1} were attributed to the stretching vibration of the (–C–O–C–) group in the ester bond of PES polymer. The peaks at 1033 and 918 cm^{-1} are due to the (–O–C–C–) stretching vibrations and (–C–OH) bending in the carboxylic acid groups of PES, respectively. Furthermore, the peaks at 2962 cm^{-1} correspond to the asymmetric stretching vibration, while 1381 cm^{-1} corresponds to the symmetric deformational vibrations of the – CH_2 – groups present in the main carbon chain of PES polymer [38].

In order to determine an optimized synthesis temperature and time, pure PES products were characterized by ^1H NMR spectroscopy at room temperature in DMSO-d_6 . Chemical shifts are reported in ppm (δ scale) relative to tetramethylsilane (TMS). Approximately 1%–5% w/v of pure PES polymer solutions were used for the ^1H NMR measurements. The degree of polymerization, or number of units, can be determined by comparing the relative proton signal intensity of a known moiety (typically an end group (s) with a known number of protons) to the proton signal intensity of the repeating unit in the polymer chain [34, 39]. The molecular weight of pure PES was probed as a function of increasing polycondensation time. The optimal polymerization reaction time was estimated by setting up the polymerization reaction at 170°C under magnetic stirring with samples extracted every 5 h for 60 h. The extracted samples were analyzed using NMR and GPC. Figure 2 shows the partial ^1H NMR spectrum for pure PES produced under these conditions for 10 h. The ^1H NMR spectra show signals assigned to the end group as well as the repeating units in the polymer chain. The singlet at 4.21 (δH^c) ppm was assigned to the methylene protons on the ethylene glycol monomers in the repeating unit. The singlet at 2.57 (δH^d) ppm was assigned to the methylene protons on the succinic acid monomers in the repeating unit [40]. The

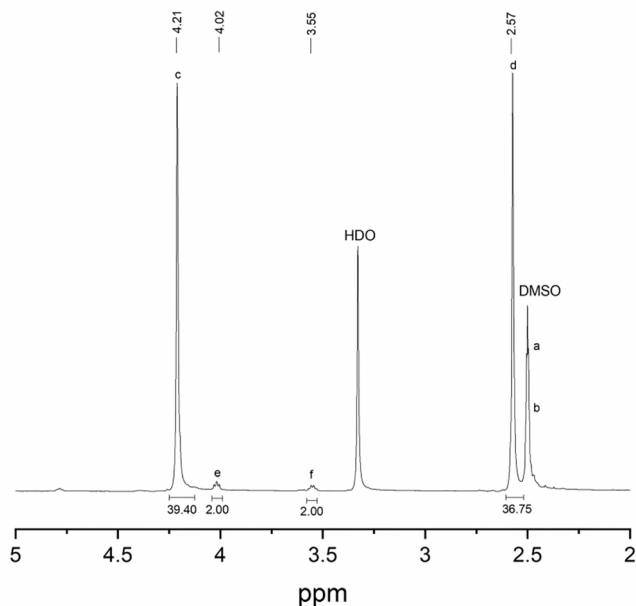


FIGURE 2 | ^1H NMR spectra of pure PES polymer synthesized at 170°C for 10 h.

triplet signals observed at 4.02 (δH^e) and 3.55 (δH^f) ppm can be assigned to the CH_2 protons on the end group of succinate end group monomers [41]. Some overlapping signals between 2.46 and 2.53 ppm (δH^a and δH^b) may be assigned to the methylene protons in the repeating unit of the PES polymer; however, these are ignored as they majorly overlap with the solvent peaks. ^1H NMR of pure succinic acid and ethylene glycol monomers differ greatly from the ^1H NMR of pure PES, indicating the formation of polymer bonds and repeating units. The ^1H NMR spectra of pure succinic acid monomer in $\text{DMSO}-d_6$ show singlets at 12.2 and 2.4 ppm representing the carboxylic acid group and CH_2 protons, respectively. Additionally, the ^1H NMR for pure ethylene glycol shows two singlet peaks at 3.3 ppm corresponding to the CH_2 protons and 4.5 ppm assigned to the OH groups.

To further analyze the polymerization progression with reaction time, the monomer to polymer conversion was calculated at each hour. This was determined by comparing specific monomer proton integrals with the corresponding proton integrals in the repeating unit. According to Figure 3, up to 91% of ethylene glycol and succinic acid monomers are converted to polyethylene succinate as the synthesis time is increased. In addition, the NMR and GPC analyses demonstrate that the molecular weight gradually increases with synthesis time due to the step-growth mechanism. The data indicate that the polycondensation method produced relatively low molecular weight polyester chains from initially $M_n = 275$ to $M_n = 1359 \text{ g mol}^{-1}$ after 60 h; low molecular weights are routinely observed for step-growth polycondensation polymerization unless very high conversions are attained because the condensation leads to the formation of dimers, then trimers, oligomers, and eventually long-chain polymers [42]. In our case, 1–8 repeat units are incorporated into the polymer chains. There is a general increase in molecular weight and monomer conversion as the polycondensation reaction time increases, with a significant increase in monomer conversion and molecular weight after 10 h. However, the monomer conversion after 60 h is only 15% higher than conversion

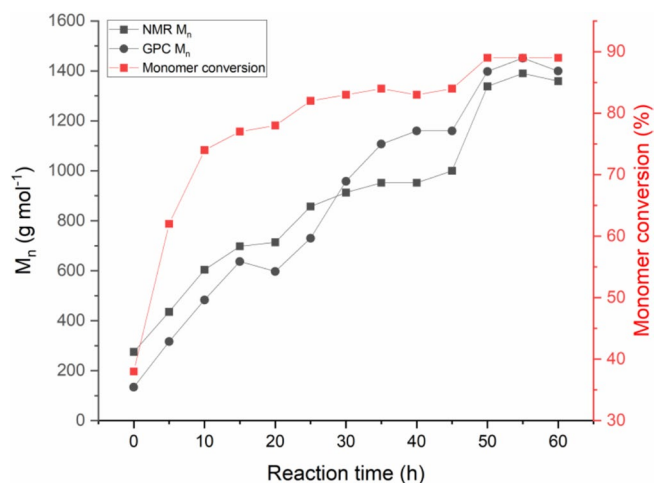


FIGURE 3 | Monomer conversion data obtained from NMR analysis changing with reaction time and molecular weight data obtained from NMR and GPC of pure PES polymer chains as a function of reaction time. [Color figure can be viewed at wileyonlinelibrary.com]]

after 10 h, leading to diminishing gains in conversion efficiency. The molecular weight of the polyesters was also measured using GPC with respect to polycondensation reaction time. Similar to NMR, the GPC data showed a gradual increase in molecular weight as the reaction time increases. The polymer M_n data obtained from GPC are comparable to the molecular weight data derived from NMR, with M_n ranging from 134 to 1399 g mol^{-1} corresponding to 1–8 repeat units. After 50 h of reaction time, both GPC and NMR show negligible differences in the molecular weight despite further heating. However, the molecular weight data obtained from GPC has a strong dependence on the calibrant (typically polystyrene) which can be a hindrance as it is assumed that the measured polymer and the standard have the same hydrodynamic radii at equivalent molecular weight. Hence, the underlying principle of the technique is separation on the basis of polymer hydrodynamic volume instead of molecular weight [43, 44]. In comparison, ^1H NMR spectroscopy is our primary quantitative method for analysis without the need for calibration [45].

The pure PES synthesis produced a yellow/brown, waxy polymer from the transparent reactants, which indicates the polycondensation of the initial monomers and the formation of the polyester molecules. S1 confirms a gradual yellow/brown change from the transparent reactants over 60 h. The final pure PES product is a thermoplastic, which can be heated to become highly viscous and subsequently cooled to reshape. The mechanical properties of the pure PES polymer were measured using a shore A hardness probe on 25 mm thick PES samples that were cooled to room temperature. Ethylene glycol and succinic acid monomers were polymerized at 170°C , and samples were extracted from the batch every hour for 24 h. The surface hardness of each extracted sample is shown in Figure 4. We observed a significant peak in surface hardness of the pure PES polymers at Hour 10, which showed a value of 90 on the Shore A hardness scale. Below 10 h of heating, the co-polymers are not fully reacted, and the polymer is a soft, waxy material. After 10 h of reaction time, the surface hardness of the PES material stays constant despite prolonged polymerization time. We identified 10 h to be an optimal polymerization time

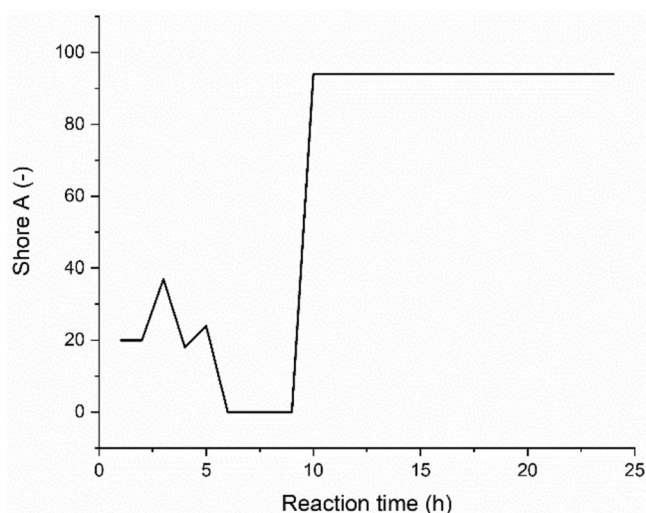


FIGURE 4 | Surface hardness of PES in response to the reaction time of polymerization.

for the synthesis of a polyethylene succinate matrix as it presents good monomer conversion and mechanically hard polyesters with sufficient molecular weights. In addition, extended heating periods at high temperatures have the potential to destabilize the BHF suspension. Having said this, the polymers produced below 150°C for a period of 10h have a brittle structure and can easily fracture.

Based on the identified 10h and 170°C synthesis conditions for the PES polymer matrix, the polycondensation reaction was repeated with a barium hexaferrite-based ferrofluid where the magnetic nanoparticles are stabilized using CTAB surfactant and suspended in ethylene glycol. This ethylene glycol ferrofluid reacted with succinic acid to produce a PES/BHF polymer composite exhibiting magnetic properties from the suspended nanoplatelets. Here, the ethylene glycol-suspended barium hexaferrite magnetic nanoparticles react with the succinic acid to produce a polyethylene succinate polymer matrix. The BHF nanoparticles are evenly dispersed within this polymer matrix once the polymer composite is allowed to cool. The thermal stability of the synthesized PES/BHF polymer composite was measured using TGA (Mettler Toledo). This was done by heating the PES/BHF samples from 25°C to 600°C at 10°C min⁻¹ in air with a gas flow of 100 mL/min. The TGA analysis in Figure 5 shows the thermal degradation of synthesized PES/BHF polymer composites for varying barium hexaferrite nanoparticle concentrations of 10, 30, and 60 mg/mL. The TGA curves for the three concentrations of the PES/BHF polymer composites start decomposing between 200°C and 330°C with approximately 20% weight loss. Subsequently, a second decomposing step was between 320°C and 420°C with a weight loss of around 75% for 60 mg/mL and approximately 85% for 30 and 10 mg/mL. A third decomposition step can be identified between 400°C and 480°C with a total weight loss of 95.50% for 60 mg/mL, 98.62% for 30 mg/mL, and 99.08% for 10 mg/mL. Therefore, a 60 mg/mL concentrated PES/BHF polymer composite contains approximately 4.50 wt% BHF nanoparticles, a 30 mg/mL PES/BHF composite contains 1.38 wt% BHF nanoparticles, and a 10 mg/mL PES/BHF composite contains 0.92 wt% BHF nanoparticles by weight. These results also confirm that a polymerization temperature higher than 200°C is unsuitable for this reaction as it may lead to the

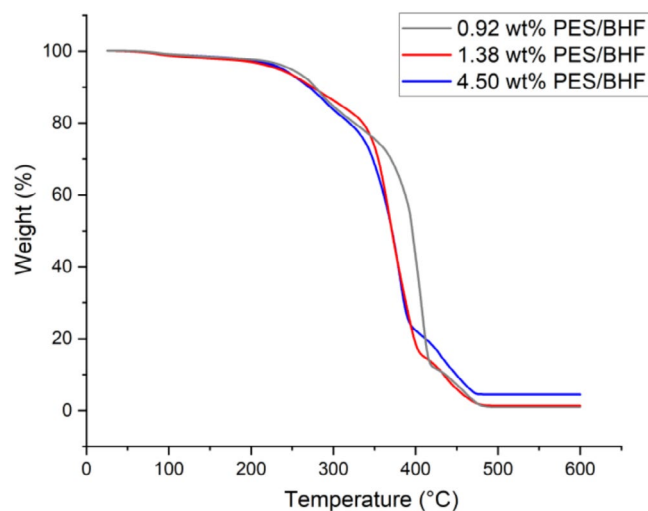


FIGURE 5 | TGA analysis of PES/BHF polymer composite matrix at 0.92 wt %, 1.38, and 4.50 wt% PES/BHF. [Color figure can be viewed at [wileyonlinelibrary.com](https://onlinelibrary.wiley.com/doi/10.1002/app.56984)]

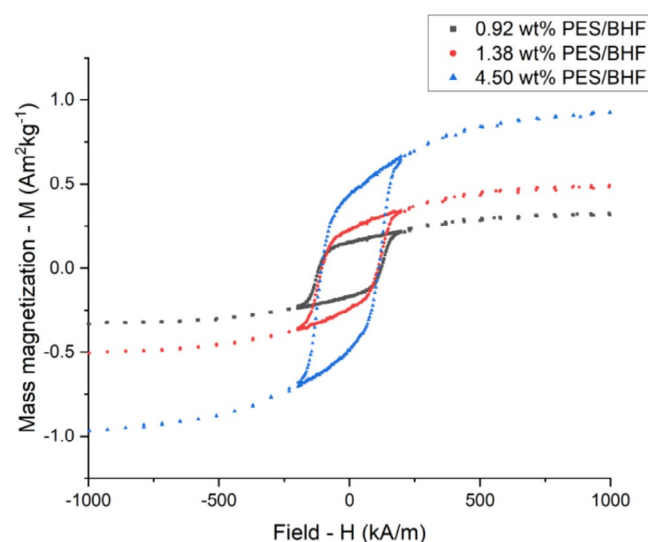


FIGURE 6 | Mass magnetization—M against applied field—H of BHF nanoparticles embedded in a PES polymer matrix at concentrations of 0.92 wt%, 1.38 wt%, and 4.50 wt% PES/BHF. [Color figure can be viewed at [wileyonlinelibrary.com](https://onlinelibrary.wiley.com/terms-and-conditions)]

decomposition of the polyester chains, decreasing the molecular weight by the thermal degradation process. Thermal analysis of the polymer composites confirms the incorporation of BHF nanoparticles in the PES polymer matrix as constant mass is obtained after prolonged heating at a temperature of 600°C, indicating the presence of BHF nanoparticles after complete polymer degradation. Subsequently, magnetic properties of the PES/BHF products were measured using VSM (LakeShore 7400) for the isotopically dispersed nanoparticles. The VSM samples were prepared by casting 0.92 wt%, 1.38 wt%, and 4.5 wt% concentrations of PES/BHF polymers at 170°C into a brass cylinder mold and allowing them to cool down to room temperature. The magnetic properties of the solid polymer composites were measured at excitation fields between -1000 and 1000 kA m⁻¹. Figure 6 shows the magnetic hysteresis loops of the PES/BHF polymer composites concentrations. The hysteresis loops of all

three concentrations are typical of a hard BHF ferrimagnetic material with a constant coercivity $H_c = 120 \text{ kA m}^{-1}$. Magnetic saturation— M_s and remanence— M_r values of the three PES/BHF polymer composites vary with particle load in the polymer matrix. The saturation and remanence values of the composites increase with increasing BHF particle concentrations, with 4.5 wt% showing magnetic saturation $M_s = 0.93 \text{ Am}^2 \text{ kg}^{-1}$ and magnetic remanence $M_r = 0.45 \text{ Am}^2 \text{ kg}^{-1}$. On the other hand, the 1.28 wt% concentrated PES/BHF polymer showed $M_s = 0.48 \text{ Am}^2 \text{ kg}^{-1}$ and $M_r = 0.24 \text{ Am}^2 \text{ kg}^{-1}$, while the 0.92 wt% PES/BHF polymer showed $M_s = 0.32 \text{ Am}^2 \text{ kg}^{-1}$ and $M_r = 0.16 \text{ Am}^2 \text{ kg}^{-1}$. The weight-specific remanence and magnetic saturation values are lower than pure BHF nanoparticle powders which have reported values of up to $10.4 \text{ mA m}^2 \text{ g}^{-1}$ for remanence and $32.8 \text{ mA m}^2 \text{ g}^{-1}$ for saturation. This is mainly reflective of the relatively low nanoparticle-to-polymer ratio in the PES/BHF composite as shown by the TGA results. However, the M_r/M_s ratios and H_c are the same for all three samples, indicating the absence of a magnetic interaction between the BHF nanoparticles in the PES/BHF composites [24].

The synthesized PES/BHF composite was microscopically analyzed using TEM. The composite was heated to 170°C and cast into a cylinder mold upon cooling to room temperature. The cast polymer cylinders were sectioned by ultramicrotomy to 70–200 nm thickness wedged slices and cooled on water droplets, which enabled overcoming compression during sectioning as well as improved adhesion to a carbon copper TEM grid support. Figure 7 shows the TEM results for the 60 mg/mL polymerized ferrofluid. The TEM shows BHF nanoparticles embedded throughout the transparent PES polymer matrix, with most of the BHF nanoparticles lying flat as opposed to perpendicular to the TEM grid. However, the BHF nanoparticles are prone to aggregation due to the strong magnetic dipole–dipole interactions between the BHF nanoparticles [21]. On the other hand, the

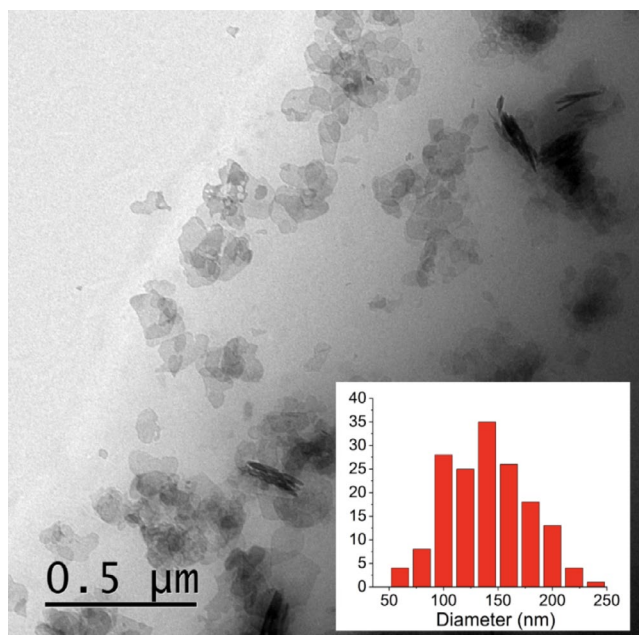


FIGURE 7 | TEM image of isotropically dispersed BHF magnetic nanoparticles embedded in a PES polymer matrix with MNP size distribution (inset). [Color figure can be viewed at [wileyonlinelibrary.com](https://onlinelibrary.wiley.com)]

TEM scan also shows signs of aggregated BHF nanoparticles, which could have occurred during the sliced sample preparation, for which reason a size distribution was determined for the pure ethylene glycol ferrofluid batch in the Figure 7 inset. In order to determine particle concentration and identify if the BHF nanoparticles are dispersed homogeneously within the matrix, the density of sliced cylindrically cast PES/BHF samples was measured across the cylinder length. The density of pure PES polymer was measured as 1.26 g/cm^3 , and increased to a density of 1.38 g/cm^3 with a standard deviation of 0.03 for PES/BHF [46]. The density of the pure polymer increases by 0.12 g/cm^3 as the embedded BHF nanoparticles are introduced. **Supporting Information** further demonstrates a homogeneous dispersion of the sliced cylindrically cast samples based on a dense Energy-Dispersive X-ray (EDX) signal. Based on the characterized and optimized PES/BHF, future work will identify biodegradable properties which, coupled with the controlled magnetic properties, may prove beneficial in many fields such as drug delivery, tissue engineering, and functional shielding materials. On the other hand, further improvements with respect to composite filler content are expected up to 50 wt%.

4 | Conclusion

We developed a new polyethylene succinate (PES) hard magnetic polymer matrix composite (PMC) with a high filler content of up to 4.5 wt% embedded with barium hexaferrite (BHF) magnetic nanoparticles, representing a significant increase compared to previous reports on barium hexaferrite-based polymer composites. This report thoroughly discusses a catalyst-free polycondensation reaction between ethylene glycol and succinic acid, along with the optimization of synthesis time and temperature. These optimizations ensure a complete and successful polycondensation reaction between the monomers, producing a PES polymer matrix with robust mechanical and thermal properties. Fourier Transform Infrared (FTIR) spectroscopy, Nuclear Magnetic Resonance (NMR) spectroscopy, Gel Permeation Chromatography (GPC), and surface hardness measurements were used to chemically and mechanically characterize the pure PES polymer matrix. This was followed by the polymerization of a CTAB-stabilized, ethylene glycol-based ferrofluid with dispersed barium hexaferrite magnetic nanoparticles. The ferrofluid was polymerized using the same catalyst-free polycondensation reaction, producing a magnetic polymer composite with homogeneously embedded isotropic barium hexaferrite nanoparticles throughout the PES matrix. We magnetically characterized this PMC using a Vibrating-Sample Magnetometer (VSM) to observe a hysteresis loop indicative of the hard magnetic properties of BHF nanoparticles, confirming the fully dispersed synthesis of a PMC with hard magnetic properties and potential biodegradability due to the PES matrix. The PMC's high filler content and thermal stability were confirmed via Thermogravimetric Analysis (TGA), while density measurements indicated the distribution of magnetic nanoparticles. Transmission Electron Microscopy (TEM) was used to observe the BHF magnetic nanoparticles embedded within the PES polymer matrix and to assess any aggregation that may have resulted from magnetic particle interactions. Although our density measurements indicate reasonably homogeneous dispersion of BHF nanoparticles in the PES matrix, advanced methods to determine stability with greater accuracy

are needed. Future work will examine the dispersion stability of higher ferrofluid concentrations and the rheological properties at high temperatures of PES/BHF samples with higher filler content. Additionally, three-dimensional (3D) manufacturing of magnetic structures will be pursued.

Author Contributions

Y. Ahmed: formal analysis (equal), investigation (lead), writing – original draft (lead). **B. D. Ward:** conceptualization (equal), formal analysis (equal), writing – review and editing (equal). **J. Steer:** investigation (equal). **D. Zabek:** conceptualization (lead), formal analysis (lead), funding acquisition (lead), investigation (equal), methodology (equal), project administration (lead), resources (lead), supervision (lead), validation (lead), visualization (supporting), writing – original draft (supporting), writing – review and editing (lead).

Acknowledgments

This research received funding from the Royal Academy of Engineering (RAEng) under the Research Fellowship Program Number RF\201819\18\202 and Cardiff University for a research infrastructure grant.

Conflicts of Interest

The authors declare no conflicts of interest.

Data Availability Statement

The data that support the findings of this study are available from the corresponding author upon reasonable request.

References

1. R.-M. Wang, S.-R. Zheng, and Y.-P. Zheng, *Polymer Matrix Composites and Technology* (Elsevier, 2011).
2. X. Wei, M.-L. Jin, H. Yang, X.-X. Wang, Y.-Z. Long, and Z. Chen, “Advances in 3D Printing of Magnetic Materials: Fabrication, Properties, and Their Applications,” *Journal of Advanced Ceramics* 11, no. 5 (2022): 665–701, <https://doi.org/10.1007/s40145-022-0567-5>.
3. W. Li, H. Gu, Z. Liu, H. Zhang, L. Jiang, and X. Zhou, “Research Progress in the Synthesis and Application of Magnetic Self-Healing Polymer Composites,” *European Polymer Journal* 202 (2024): 112633, <https://doi.org/10.1016/j.eurpolymj.2023.112633>.
4. A. Sharma, D. Mangla, and S. A. Chaudhry, “Recent Advances in Magnetic Composites as Adsorbents for Wastewater Remediation,” *Journal of Environmental Management* 306 (2022): 114483, <https://doi.org/10.1016/j.jenvman.2022.114483>.
5. S. Gil and J. F. Mano, “Magnetic Composite Biomaterials for Tissue Engineering,” *Biomaterials Science* 2, no. 6 (2014): 812–818, <https://doi.org/10.1039/C4BM00041B>.
6. E. Aram and H. A. Khonakdar, “Preparation and Evaluation of Polyethylene Glycol Conjugated Polyethylene Imine-Coated Magnetic Nanoparticles for Paclitaxel Delivery to Cervical Cancer Cells,” *Polymers for Advanced Technologies* 35, no. 10 (2024): e6601, <https://doi.org/10.1002/pat.6601>.
7. J. Zhang, Y. Zhang, L. Cao, J. Wang, and G. Tian, “Preparation, Characterization and Adsorption Application of Magnetic Nanocomposite Fe₂O₃/SBA-15/HKUST-1,” *Inorganic Chemistry Communications* 161 (2024): 112147, <https://doi.org/10.1016/j.inoche.2024.112147>.
8. E. Aram, H. Sadeghi-Abandansari, F. Radmanesh, et al., “Shell-Sheddable and Charge Switchable Magnetic Nanoparticle as pH-Sensitive Nanocarrier for Targeted Drug Delivery Applications,”

Polymers for Advanced Technologies 35, no. 4 (2024): e6366, <https://doi.org/10.1002/pat.6366>.

9. E. Aram, M. Moeni, R. Abedizadeh, et al., “Smart and Multifunctional Magnetic Nanoparticles for Cancer Treatment Applications: Clinical Challenges and Future Prospects,” *Nanomaterials* 12, no. 20 (2022): 3567, <https://doi.org/10.3390/nano12203567>.

10. J. Ramos, A. Millán, and F. Palacio, “Production of Magnetic Nanoparticles in a Polyvinylpyridine Matrix,” *Polymer* 41, no. 24 (2000): 8461–8464, [https://doi.org/10.1016/S0032-3861\(00\)00272-X](https://doi.org/10.1016/S0032-3861(00)00272-X).

11. F. L. Matthews and R. D. Rawlings, *Composite Materials* (Elsevier, 1999), <https://doi.org/10.1016/C2013-0-17714-8>.

12. W. Jiang, H. Zhu, C. Guo, et al., “Poly(Methyl Methacrylate)-Coated Carbonyl Iron Particles and Their Magnetorheological Characteristics: Magnetorheological Characteristics of PMMA-Coated CI Particles,” *Polymer International* 59, no. 7 (2010): 879–883, <https://doi.org/10.1002/pi.2794>.

13. Z. Guo, L. L. Henry, V. Palshin, and E. J. Podlaha, “Synthesis of Poly(Methyl Methacrylate) Stabilized Colloidal Zero-Valence Metallic Nanoparticles,” *Journal of Materials Chemistry* 16, no. 18 (2006): 1772–1777, <https://doi.org/10.1039/B515565G>.

14. T. Gong, D. Yang, J. Hu, W. Yang, C. Wang, and J. Q. Lu, “Preparation of Monodispersed Hybrid Nanospheres With High Magnetite Content From Uniform Fe₃O₄ Clusters,” *Colloids and Surfaces A: Physicochemical and Engineering Aspects* 339, no. 1–3 (2009): 232–239, <https://doi.org/10.1016/j.colsurfa.2009.02.034>.

15. S. Akgöl, Y. Kaçar, A. Denizli, and M. Y. Arıca, “Hydrolysis of Sucrose by Invertase Immobilized Onto Novel Magnetic Polyvinylalcohol Microspheres,” *Food Chemistry* 74, no. 3 (2001): 281–288, [https://doi.org/10.1016/S0308-8146\(01\)00150-9](https://doi.org/10.1016/S0308-8146(01)00150-9).

16. J. Yang, T.-I. Lee, J. Lee, et al., “Synthesis of Ultrasensitive Magnetic Resonance Contrast Agents for Cancer Imaging Using PEG-Fatty Acid,” *Chemistry of Materials* 19, no. 16 (2007): 3870–3876, <https://doi.org/10.1021/cm070495s>.

17. S. S. Banerjee and D.-H. Chen, “Magnetic Nanoparticles Grafted With Cyclodextrin for Hydrophobic Drug Delivery,” *Chemistry of Materials* 19, no. 25 (2007): 6345–6349, <https://doi.org/10.1021/cm702278u>.

18. F. Liu, Q.-Q. Ni, and Y. Murakami, “Preparation of Magnetic Polyvinyl Alcohol Composite Nanofibers With Homogenously Dispersed Nanoparticles and High Water Resistance,” *Textile Research Journal* 83, no. 5 (2013): 510–518, <https://doi.org/10.1177/0040517512444334>.

19. E. L. Mayes, F. Vollrath, and S. Mann, “Fabrication of Magnetic Spider Silk and Other Silk-Fiber Composites Using Inorganic Nanoparticles,” *Advanced Materials* 10, no. 10 (1998): 801–805, [https://doi.org/10.1002/\(SICI\)1521-4095\(199807\)10:10<801::AID-ADMA801>3.0.CO;2-I](https://doi.org/10.1002/(SICI)1521-4095(199807)10:10<801::AID-ADMA801>3.0.CO;2-I).

20. X. Liu, Y. Guan, Z. Ma, and H. Liu, “Surface Modification and Characterization of Magnetic Polymer Nanospheres Prepared by Miniemulsion Polymerization,” *Langmuir* 20, no. 23 (2004): 10278–10282, <https://doi.org/10.1021/la0491908>.

21. P. Hribar Boštjančič, M. Tomšič, A. Jamnik, D. Lisjak, and A. Mertelj, “Electrostatic Interactions Between Barium Hexaferrite Nanoplatelets in Alcohol Suspensions,” *Journal of Physical Chemistry C* 123, no. 37 (2019): 23272–23279, <https://doi.org/10.1021/acs.jpcc.9b07455>.

22. J. J. Went, G. W. Rathenau, E. W. Gorter, and G. W. van Oosterhout, “Hexagonal Iron-Oxide Compounds as Permanent-Magnet Materials,” *Physics Review* 86, no. 3 (1952): 424–425, <https://doi.org/10.1103/PhysRev.86.424.2>.

23. R. C. Pullar, “Hexagonal Ferrites: A Review of the Synthesis, Properties and Applications of Hexaferrite Ceramics,” *Progress in Materials Science* 57, no. 7 (2012): 1191–1334, <https://doi.org/10.1016/j.pmatsci.2012.04.001>.

24. G. Ferk, P. Krajnc, A. Hamler, et al., "Monolithic Magneto-Optical Nanocomposites of Barium Hexaferrite Platelets in PMMA," *Scientific Reports* 5, no. 1 (2015): 11395, <https://doi.org/10.1038/srep11395>.
25. D. Lisjak and A. Mertelj, "Anisotropic Magnetic Nanoparticles: A Review of Their Properties, Syntheses and Potential Applications," *Progress in Materials Science* 95 (2018): 286–328, <https://doi.org/10.1016/j.pmatsci.2018.03.003>.
26. Ž. Gregorin, N. Sebastián, N. Osterman, P. Hribar Boštjančič, D. Lisjak, and A. Mertelj, "Dynamics of Domain Formation in a Ferromagnetic Fluid," *Journal of Molecular Liquids* 366 (2022): 120308, <https://doi.org/10.1016/j.molliq.2022.120308>.
27. S. Gao, M. Fleisch, R. A. Rupp, et al., "Magnetically Tunable Optical Diffraction Gratings Based on a Ferromagnetic Liquid Crystal," *Optics Express* 27, no. 6 (2019): 8900–8911, <https://doi.org/10.1364/OE.27.008900>.
28. J. Hu, T. Gorsak, E. Martín Rodríguez, et al., "Magnetic Nanoplatelets for High Contrast Cardiovascular Imaging by Magnetically Modulated Optical Coherence Tomography," *ChemPhotoChem* 3, no. 7 (2019): 529–539, <https://doi.org/10.1002/cptc.201900071>.
29. J. Philip, "Magnetic Nanofluids (Ferrofluids): Recent Advances, Applications, Challenges, and Future Directions," *Advances in Colloid and Interface Science* 311 (2023): 102810, <https://doi.org/10.1016/j.cis.2022.102810>.
30. Y. Ahmed, A. Paul, P. Hribar Boštjančič, A. Mertelj, D. Lisjak, and D. Zabek, "Synthesis of Barium Hexaferrite Nano-Platelets for Ethylene Glycol Ferrofluids," *Journal of Materials Chemistry C* 11, no. 45 (2023): 16066–16073, <https://doi.org/10.1039/D3TC03833E>.
31. D. Lisjak and M. Drogenik, "Chemical Substitution—An Alternative Strategy for Controlling the Particle Size of Barium Ferrite," *Crystal Growth & Design* 12, no. 11 (2012): 5174–5179, <https://doi.org/10.1021/cg301227r>.
32. M. M. Abdelghafour, Á. Orbán, Á. Deák, et al., "The Effect of Molecular Weight on the Solubility Properties of Biocompatible Poly(Ethylene Succinate) Polyester," *Polymers* 13, no. 16 (2021): 2725, <https://doi.org/10.3390/polym13162725>.
33. X. Jiang, Y. Hu, Z. Meng, W. Yang, and F. Shen, "Solubility of Succinic Acid in Different Aqueous Solvent Mixtures: Experimental Measurement and Thermodynamic Modeling," *Fluid Phase Equilibria* 341 (2013): 7–11, <https://doi.org/10.1016/j.fluid.2012.12.018>.
34. J. U. Izunobi and C. L. Higginbotham, "Polymer Molecular Weight Analysis by ¹H NMR Spectroscopy," *Journal of Chemical Education* 88, no. 8 (2011): 1098–1104, <https://doi.org/10.1021/ed100461v>.
35. J. Wang, W. Chen, L. Bai, Y. Tian, and X. Ba, "Synthesis of High Regular Poly (Ethylene Succinate) by Adding Oxalic Acid in Poly-Condensation System: Suppressing Etherification Side Reaction," *Polymer* 16, no. 263 (2022): 125527, <https://doi.org/10.1016/j.polymer.2022.125527>.
36. T. Mitra, G. Sailakshmi, A. Gnanamani, and A. B. Mandal, "Studies on Cross-Linking of Succinic Acid With Chitosan/Collagen," *Materials Research* 16, no. 4 (2013): 755–765, <https://doi.org/10.1590/S1516-14392013005000059>.
37. K. Krishnan and R. S. Krishnan, "Infrared Spectra of Ethylene Glycol," *Proceedings of the Indian Academy of Sciences-Section A* 64, no. 2 (1966): 111, <https://doi.org/10.1007/BF03047675>.
38. Y. J. Phua, W. S. Chow, and Z. A. Mohd Ishak, "The Hydrolytic Effect of Moisture and Hygrothermal Aging on Poly(Butylene Succinate)/Organo-Montmorillonite Nanocomposites," *Polymer Degradation and Stability* 96, no. 7 (2011): 1194–1203, <https://doi.org/10.1016/j.polymdegradstab.2011.04.017>.
39. P. A. Mirau, "NMR Characterisation of Polymers," in *Polymer Characterisation*, ed. B. J. Hunt and M. I. James (Springer Netherlands, 1993), 37–68, https://doi.org/10.1007/978-94-011-2160-6_3.
40. J.-B. Zeng, Y.-D. Li, W.-D. Li, K.-K. Yang, X.-L. Wang, and Y.-Z. Wang, "Synthesis and Properties of Poly(Ester Urethane)s Consisting of Poly(L-Lactic Acid) and Poly(Ethylene Succinate) Segments," *Industrial and Engineering Chemistry Research* 48, no. 4 (2009): 1706–1711, <https://doi.org/10.1021/ie801391m>.
41. A. Oishi, M. Zhang, K. Nakayama, T. Masuda, and Y. Taguchi, "Synthesis of Poly(Butylene Succinate) and Poly(Ethylene Succinate) Including Diglycollate Moiety," *Polymer Journal* 38, no. 7 (2006): 710–715, <https://doi.org/10.1295/polymj.PJ2005206>.
42. A. Ravve, *Principles of Polymer Chemistry* (Springer New York, 2012), <https://doi.org/10.1007/978-1-4614-2212-9>.
43. M. Wong, J. Hollinger, L. M. Kozycz, et al., "An Apparent Size-Exclusion Quantification Limit Reveals a Molecular Weight Limit in the Synthesis of Externally Initiated Polythiophenes," *ACS Macro Letters* 1, no. 11 (2012): 1266–1269, <https://doi.org/10.1021/mz300333f>.
44. J. P. Sibilía, *A Guide to Materials Characterization and Chemical Analysis*, 2nd ed. (VCH, 1996).
45. H. G. Barth and J. W. Mays, "Modern Methods of Polymer Characterization," in *Chemical Analysis* (J. Wiley & sons: New York Chichester Brisbane, 1991).
46. L. Aliotta, M. Seggiani, A. Lazzeri, V. Gigante, and P. Cinelli, "A Brief Review of Poly (Butylene Succinate) (PBS) and Its Main Copolymers: Synthesis, Blends, Composites, Biodegradability, and Applications," *Polymers* 14, no. 4 (2022): 844, <https://doi.org/10.3390/polym14040844>.